Society of Medical Education & Research

2025, Volume 5, Issue 2, Page No: 138-158
ISSN: 3108-4834

Archive of International Journal of Cancer and Allied Science

# CircAXIN1-Encoded AXIN1-295aa Activates Wnt/β-Catenin Signaling to Drive Gastric Cancer Progression

**William James Clark[1], Charlotte Rose Davies[1]*, Simon Peter Hall[1]**

[1]Auckland Cancer Society Research Centre, University of Auckland, Auckland, New Zealand.

***E-mail** ✉ w.clark.auckland@outlook.com

## Abstract

Circular RNAs (circRNAs), which belong to the category of non-coding RNAs, play an important role in the development and spread of cancer. They are thought to function primarily as sponges for microRNAs or as platforms that facilitate interactions with protein complexes, yet their complete spectrum of biological roles is still not fully understood. In recent studies, certain circRNAs have been discovered to possess the ability to encode proteins .To determine the involvement of circular RNAs in gastric cancer (GC), high-throughput sequencing was conducted on five matched pairs of tumor and adjacent normal tissues. This analysis identified circAXIN1 as a significantly dysregulated circRNA with the potential to produce a previously unknown protein. The translational capability of circAXIN1 was verified by generating FLAG-labeled circRNA expression constructs and performing Western blotting, mass spectrometry, and dual-luciferase reporter assays. Functional gain- and loss-of-expression approaches were subsequently employed to assess the effects of circAXIN1 and its translated product, AXIN1-295aa, on GC cell growth, motility, invasiveness, and metastatic capacity in both cellular and animal models. The competitive binding relationship between AXIN1-295aa and adenomatous polyposis coli (APC) was analyzed using co-immunoprecipitation techniques. Activation of the Wnt pathway was evaluated through Top/Fopflash reporter assays in combination with quantitative RT-PCR, Western blot analysis, immunofluorescence microscopy, and chromatin immunoprecipitation assays.CircAXIN1 is markedly upregulated in gastric cancer (GC) tissues relative to matched adjacent noncancerous gastric samples. It was found to translate a previously unrecognized 295–amino acid protein, designated AXIN1-295aa. Ectopic expression of circAXIN1 significantly promotes GC cell proliferation, migration, and invasiveness, whereas silencing circAXIN1 suppresses these malignant phenotypes both in vitro and in vivo. Mechanistically, AXIN1-295aa competes with adenomatous polyposis coli (APC) for binding, thereby impairing the integrity of the Wnt signaling destruction complex. As a result, stabilized β-catenin accumulates and translocates into the nucleus, where it associates with TCF binding elements in target gene promoters to activate downstream transcriptional programs. CircAXIN1 was shown to produce a newly characterized protein, AXIN1-295aa, which exerts tumor-promoting effects by stimulating Wnt pathway activity. Through this mechanism, AXIN1-295aa contributes to the development and advancement of gastric cancer, indicating its promise as a novel molecular target for therapeutic intervention.

**Keywords:** Wnt, AXIN1, circRNA, Translation

## Introduction

Circular RNAs (circRNAs) represent a distinct group of RNA transcripts distinguished by a covalently closed circular configuration, lacking both 5′–3′ directionality and a polyadenylated tail [1]. The majority of circRNAs arise through back-splicing of exonic sequences, an atypical form of RNA splicing [2, 3]. Their expression patterns are highly specific to tissue type, developmental stage, and disease state [4]. Functionally, circRNAs have been reported to serve as microRNA decoys, regulators of transcription, and molecular platforms that facilitate protein interactions or subcellular localization [5]. More recent studies have revealed that certain circRNAs possess translational capability [6-8], a finding that is

Access this article online https://smerpub.com/

**Received:** 23 August 2025; **Accepted:** 21 November 2025



**How to cite this article:** Clark WJ, Davies CR, Hall SP. Outcomes of Everolimus Combined with Exemestane in HR-Positive Metastatic Breast Cancer after CDK4/6 Inhibitor Exposure. Arch Int J Cancer Allied Sci. 2025;5(2):1138-58. https://doi.org/10.51847/fhyhFRrfxD

supported by the fact that many circRNAs are exon-derived and predominantly localized within the cytoplasm [9]. Notably, Zhang and colleagues demonstrated that several circRNAs can be translated into proteins with tumor-suppressive functions in glioblastoma [10].

Gastric cancer (GC) remains a leading cause of cancer-related mortality in China and worldwide, largely due to the absence of effective strategies for early detection [11]. Owing to their exceptional stability, circRNAs have emerged as promising molecular candidates for early diagnostic biomarkers [1]. The Wnt/β-catenin signaling cascade is crucial for embryonic development, cellular differentiation, tissue homeostasis, and tumor formation [12]. Aberrations in this pathway are present in most cancers, reflecting its fundamental role in maintaining cellular viability [13]. Regulation of cytoplasmic β-catenin stability serves as a central control point in Wnt signaling [13] and is governed by the APC/AXIN destruction complex [14]. Impairment of APC [15] or AXIN [16] disrupts this complex, resulting in pathological accumulation of β-catenin. Moreover, aberrant activation of Wnt/β-catenin signaling has been documented in approximately 30–50% of GC cases [17, 18], although the precise mechanisms driving β-catenin dysregulation in GC remain poorly defined. To date, relatively few studies have investigated the functional contribution of circRNAs to GC pathogenesis [19, 20]. Elucidating how circRNAs influence the Wnt/β-catenin pathway may therefore deepen our understanding of GC molecular mechanisms and support the identification of novel early diagnostic markers.

In the present work, analysis of high-throughput sequencing data from five matched pairs of GC tissues revealed a significant upregulation of circAXIN1 in gastric tumors. We further demonstrated that circAXIN1 encodes a previously uncharacterized protein, termed AXIN1-295aa. This study aimed to clarify the interaction between AXIN1-295aa and the Wnt/β-catenin signaling pathway and to define its functional significance in the initiation and progression of gastric cancer.

## Materials and Methods

*Tissue and cell culture*

In this investigation, 63 matched sets of normal gastric tissue and gastric cancer (GC) specimens were obtained from individuals receiving treatment at Shenzhen Second People's Hospital in China. These specimens had not been exposed to any chemotherapy or radiotherapy before being surgically removed, and they were promptly stabilized in RNAlater solution (Thermo Fisher, Shanghai, China) post-operation. Every participant supplied written informed consent, while the research protocol was endorsed by the ethics committee at Shenzhen University School of Medicine.

Dr. Duane T. Smoot from Meharry Medical College in the USA generously supplied the immortalized human normal gastric epithelial cell line known as HFE-145. Sources for the gastric cancer cell lines included the American Type Culture Collection (ATCC) for AGS and the China Infrastructure of Cell Line Resources for MKN28. Additionally, the Cell Bank of the Chinese Academy of Sciences (Shanghai, China) provided the BGC-823, GES-1, NCI-N87 (N87), and SGC7901 (abbreviated as N87) lines. Cultivation of all these cell lines occurred in DMEM medium (Hyclone, Logan, Utah) enriched with 10% fetal bovine serum (FBS from Gibco), under conditions of 37 °C in a humidified incubator with 5% $CO_2$.

*Plasmids and cell transfection*

The full-length circAXIN1 tagged with 3xFLAG was chemically synthesized and inserted into the pLC5-ciR vector through EcoRI and BamHI restriction sites. This vector includes artificial flanking sequences as well as splice acceptor (SA) and splice donor (SD) elements. The 3xFLAG tag was positioned immediately upstream of the predicted stop codon within the open reading frame (ORF). A linear CMV-AXIN1-295aa overexpression plasmid was used as a positive control. Additionally, mCherry-IRES-GFP was cloned into a psin-EF2 vector. Both wild-type and mutant forms of internal ribosome entry sites (IRES115–186, IRES115–257, IRES187–257, IRES764–838, IRES689–838, and IRES689–763) were cloned into a P-Luc2-IRES-Report vector via Geneseed (Guangzhou, China). Plasmid transfections were performed on cells at 30–50% confluence using Lipofectamine™ 3000 Transfection Reagent (Invitrogen, Shanghai, China). For knockdown experiments, circAXIN1-specific siRNAs were synthesized by Geneseed (Guangzhou, China) with the following sequences: si-hsa_circAXIN1_03: AGAGTTCAGGACAGATTGA; si-hsa_circAXIN1_01: AGAGAGTTCAGGACAGATT; and si-hsa_circAXIN1_02: GAGAGTTCAGGACAGATTG . Cells at 30–50% confluence were transfected with 60 nM of these siRNAs

using Lipofectamine RNAiMAX (Invitrogen, Shanghai, China).

*RNA-sequencing assay*

RNA samples from five gastric cancer (GC) tissues and their matched adjacent normal tissues were subjected to sequencing on an Illumina Hiseq 2500 platform (Chi Biotech, Shenzhen, China). The generated reads were mapped to the human reference genome (GRCh38) using the BWA alignment tool. Circular RNAs were detected with CIRI software (version 2) and annotated according to the gene annotation file corresponding to the reference genome. Full-length sequences of the circRNAs were extracted and used as a reference for mapping the fastq reads with Bowtie2. The alignments were then converted to BAM files, sorted, and indexed, and read counts were calculated using Bedtools multiBamCov. The count data were normalized to transcripts per kilobase million (TPM), and differential expression analysis was performed using the R package limma. CircRNAs showing a fold-change greater than 2 with p-values below 0.05 were considered significantly differentially expressed.

*Real-time quantitative RT-PCR and RT-PCR*

Total RNA isolation was performed with TRIzol reagent (Invitrogen, catalog no. 251808) following the instructions provided by the manufacturer. Separation of cytoplasmic and nuclear RNA fractions was achieved using the Nuclear RNA Purification Kit (Norgen Biotek) & Cytoplasmic. To facilitate circRNA detection, linear RNAs were digested by treatment with RNase R (Geneseed, 10 U) at 37 °C for 30 min. Subsequently, purified RNA was recovered with the RNeasy MinElute Cleanup Kit (QIAGEN, catalog no. 74204). Reverse transcription and quantitative real-time PCR were carried out using GoScript™ Reverse Transcription Mix (Promega, catalog nos. A6002 and A2800). 18S rRNA and GAPDH served as endogenous reference controls.

*Western blotting*

Proteins were isolated using 2× Laemmli sample buffer (Bio-Rad) supplemented with protease inhibitor (Roche). Separation of nuclear and cytoplasmic protein fractions was performed with NE-PER™ Nuclear and Cytoplasmic Extraction Reagents (Thermo Fisher Scientific). The Western blot procedure was carried out as described previously [21]. The following antibodies were employed: Ubiquitin (cat. no. ab7780, Abcam), FLAG (cat. no. F1804, Sigma), AXIN1 (cat. no. #3323, Cell Signaling), Wnt/β-Catenin Activated Targets Antibody Sampler Kit (cat. no. #8655, Cell Signaling), HDAC (cat. no. A0238, ABclonal), AXIN1 (cat. no. A4747-01A, US Biological), β-catenin (cat. no. #8480, Cell Signaling), AXIN1 (cat. no. NBP1–31013, Novus Biologicals), Rabbit IgG control (cat. no. #3900, Cell Signaling), GSK3β (cat. no. #12456, Cell Signaling), Mouse IgG control (cat. no. #5415, Cell Signaling), and the GAPDH (cat. no. #5174, Cell Signaling).

*Mass spectrometry and co-immunoprecipitation*

Co-immunoprecipitation and immunoprecipitation experiments were carried out with the Pierce Classic Magnetic Co-IP/IP Kit (Thermo Fisher Scientific, catalog no. 88804). Lysis of cells was performed using ice-cold lysis buffer, followed by centrifugation at 13,000 g for 10 min to obtain the supernatant. Around 1000 μg of protein was then incubated overnight at 4 °C with the appropriate IP antibody (dilution 1:50) on a rotating mixer. Subsequently, 25 μL of Pierce Protein A/G Magnetic Beads were added to the antibody–antigen mixture and incubated for 1 h at room temperature. Following several washes, the bound antibody–antigen complexes were eluted using 100 μL of Elution Buffer combined with 10 μL of Neutralization Buffer. The eluted samples were then subjected to either Western blot analysis or mass spectrometry analysis performed at BGI (Shenzhen, China). To prevent detection of immunoglobulin heavy and light chains, VeriBlot for IP Detection Reagent (HRP) (Abcam, cat. no. ab131366) was employed.

*Chromatin immunoprecipitation*

The chromatin immunoprecipitation (ChIP) assay was conducted using the Magna ChIP G kit (Millipore, catalog nos. 17–409 and MAGNA0002) in accordance with the manufacturer's protocol. Following crosslinking and sonication of chromatin, 50 μL of fragmented DNA was incubated overnight at 4 °C with 20 μL of protein G magnetic beads and anti-β-catenin antibody (cat. no. #8480, dilution 1:50, Cell Signaling). As a negative control, Rabbit (DA1E) mAb IgG XP Isotype Control (cat. no. #3900, dilution 1:50, Cell Signaling) was used. Protein–DNA complexes were subsequently eluted, and purified DNA was recovered for quantitative real-time PCR (qRT-PCR) analysis. Primers targeting the promoters of Wnt signaling downstream genes (CMYC, CD44, and C-Jun) were designed such that the amplified regions included the β-catenin/TCF binding motif 5′-A/T

A/T CAAAG-3′. qRT-PCR was carried out as described earlier [21].

*Dual-luciferase reporter assay*

Fopflash and Topflash reporter plasmids were sourced from Addgene (MA, Cambridge, USA). The two predicted IRES sequences, along with their truncated versions, were cloned into the P-Luc2-IRES-Report vector (Guangzhou, Geneseed). Measurement of Firefly and Renilla luciferase activities was performed using the Dual-Glo Luciferase Assay Kit (Promega).

*Confocal immunostaining*

Cells were seeded into 35-mm petri dishes (NEST) and, after 48 hours, transfected with either circAXIN1 si1and OV-circAXIN1. As positive controls, Wnt agonist 1 (Selleckchem, cat. no. S8178) and XAV-939 (Selleckchem, cat. no. S1180) were applied at concentrations of 10 μM and 1 μM, respectively. Following fixation and permeabilization, the cells were incubated overnight at 4 °C with anti-β-catenin primary antibody (dilution 1:100, cat. no. #2677, Cell Signaling). On the following day, cells were treated for 1 hour at room temperature in the dark with Alexa Fluor® 488-conjugated anti-rabbit secondary antibody (dilution 1:500, cat. no. #4412, Cell Signaling). Nuclear staining was performed using DAPI II (Abbott Molecular, Abbott Park, Illinois). Confocal images were acquired with a ZEISS microscope.

*Immunohistochemistry*

Immunohistochemical analysis was conducted using a DAB detection kit (cat. no. ZLI-9017, ZSGB-BIO) along with a Mouse Polymer Detection Kit (cat. no. PV6002, ZSGB-BIO). Paraffin-embedded tissue sections were initially deparaffinized and rehydrated through sequential washes in xylene and graded ethanol solutions. Antigen retrieval was performed by microwaving the slides in EDTA retrieval solution (10 μM, cat. no. ZLI-9067, ZSGB-BIO) for 20 min. After cooling to room temperature and rinsing with PBS, endogenous peroxidase activity was blocked with 3% hydrogen peroxide for 10 min. Following additional washes, sections were incubated overnight at 4 °C with primary antibodies diluted 1:100 (except where noted): Ki-67 (cat. no. GB111499, Servicebio, 1:1000), TCF-1 (cat. no. #2203, Cell Signaling, 1:100), β-catenin (cat. no. #8480, Cell Signaling, 1:100), c-Jun (cat. no. #9165, Cell Signaling, 1:100), and Met (cat. no. #8198, Cell Signaling, 1:100). On the following day, slides were treated with secondary antibody for 20 min at 37 °C. Color development was achieved by adding an equal volume of DAB substrate for 10 min. Sections were then counterstained with hematoxylin after thorough washing, and finally mounted with neutral resin. Staining intensity in the sections was independently evaluated by two experienced pathologists. Intensity was graded on a 0–3 scale (0: negative; 1: weak; 2: moderate; 3: strong), while the proportion of positive cells was scored from 0 to 4 (0: none; 1: 1–25%; 2: 26–50%; 3: 51–75%; 4: 76–100%). The overall score for each section was determined by multiplying the intensity score by the percentage score.

*Prediction of protein–protein interactions and protein structure*

The open reading frame (ORF) nucleotide sequence was used to deduce the amino acid sequence of AXIN1-295aa. As described in a previous study [22], a 25-amino-acid SAMP (serine-alanine-methionine-proline) motif derived from APC directly binds to the RGS (regulators of G protein signaling) domain of AXIN1. Structural models for both AXIN1-295aa and the APC SAMP region were generated using the protein fold recognition tool PHYRE [23]. The potential interaction between AXIN1-295aa and the SAMP motif was modeled with the protein–protein docking server ZDOCK [24].

*In vitro invasion, migration, proliferation, and colony formation assays*

An EdU incorporation kit (RiboBio, Guangzhou) was employed to evaluate cellular proliferation. Forty-eight hours following transfection, the cells were processed for the assay using the method outlined in a prior publication [25]. The rate of proliferation was computed as the proportion of EdU-positive cells (appearing red) relative to the overall cell count (appearing blue).

To assess invasion and migration capabilities, sterile Transwell® inserts featuring 8.0-μm polycarbonate membranes (catalog nos. 3422 and 3428, Corning) were utilized. Post-transfection (48 hours), AGS cells designated for migration testing were exposed to mitomycin-C (10 μg/mL, Sigma, St. Louis, MO) for 1 hour at 37 °C as a pretreatment, while N87 cells skipped this step. In serum-free conditions, $5 \times 10^4$ cells were added to the top compartment. After a 24-hour period at 37 °C, cells that had traversed the membrane were fixed, hematoxylin-stained, and enumerated across five arbitrarily chosen microscopic fields.

Additionally, a scratch wound assay was carried out to gauge cell motility. Cells after transfection were placed in 6-well plates and treated with mitomycin-C (10 μg/mL, Sigma, St. Louis, MO) for 1 hour at 37 °C beforehand. At the initial time point (0 hours), a linear wound was introduced. Measurements of wound closure were taken from five selected fields at 0, 24, and 48 hours.

Colony-forming ability was used to measure long-term survival. Roughly 200 cells per well, post-transfection, were distributed into 6-well plates and grown for two weeks prior to evaluation. Triplicate replications were performed for every assay.

*In vivo metastasis and tumorigenesis assays*

In vivo experiments utilized female BALB/c athymic nude mice (4–6 weeks old) purchased from Charles River Laboratories (Beijing, China). Every animal procedure adhered strictly to the protocols approved by the Institutional Animal Care and Use Committee at Shenzhen University.

Subcutaneous xenografts were generated by injecting $5 \times 10^6$ AGS cells into the right flank of each mouse (7 animals per group). For the treatment arm, cholesterol-modified circAXIN1-siRNA (10 nmol, from Geneseed) was delivered directly into the tumors twice weekly over three weeks. Measurements of tumor size were taken every three days, followed by tumor excision for downstream analyses.

An experimental lung metastasis model was created by administering $1 \times 10^6$ AGS cells intravenously through the tail vein. Simultaneously, circAXIN1-siRNA was given systemically via tail vein injections twice per week for six weeks. Upon completion, lungs were removed and processed for hematoxylin and eosin (H&E) staining to identify and enumerate metastatic foci.

*Statistical analysis*

Statistical differences were analyzed using either Student's t-test or one-way analysis of variance (ANOVA), depending on the comparison. Results from three independent replicates are presented as mean values ± standard deviation (SD). Statistical significance was defined as a p-value less than 0.05.

## Results and Discussion

*Differential circRNA expression profile in human GC*

To investigate the expression pattern of circRNAs in gastric cancer (GC) and matched adjacent non-cancerous tissues, circRNA sequencing was conducted on RNA samples depleted of linear transcripts from five paired GC and normal tissues. RNA isolated from five pairs of human GC tissues and corresponding adjacent normal tissues was sequenced using the Illumina HiSeq 2500 platform. Alignment of the sequencing reads to the human reference genome (GRCh38) was performed with the BWA aligner. Identification of circRNAs was achieved using CIRI software (version 2). Annotation of the detected circRNAs was carried out based on the gene annotation file matched to the reference genome, followed by extraction of their full-length sequences. These full-length circRNA sequences were collectively used as a custom reference, and the original fastq reads were remapped to it with bowtie2. Read counts were then obtained using bedtools multiBamCov after converting, sorting, and indexing the bowtie2 alignments to BAM format. Normalization of count data was performed as transcripts per million (TPM), and differential expression analysis of circRNAs was conducted with the R package limma. CircRNAs exhibiting a fold change >2 and p-value <0.05 were classified as significantly differentially expressed.

Across all samples, a total of 45,783 circRNAs were detected. Among these, 79% (36,218/45,783) originated from exons, 1% (462/45,783) were intronic, 4% (1848/45,783) were intergenic, 15% (6744/45,783) showed sense overlap, and 1% (511/45,783) were antisense **(Figure 1a).** For most circRNAs, the number of back-spliced junction reads was below 100 **(Figure 1b)**. CircRNA distribution across chromosomes was uneven, with the highest number located on chromosome NC_000001.11 (chromosome 1) **(Figure 1c).** No notable differences were found in chromosomal distribution patterns between the cancer and normal groups. The majority of circRNAs had lengths shorter than 1500 nucleotides (nt) **(Figure 1d)**. The hierarchical clustering dendrogram illustrates the relationships among samples and differentially expressed circRNAs, clearly separating the expression profiles of normal and cancerous tissues **(Figure 1e).**

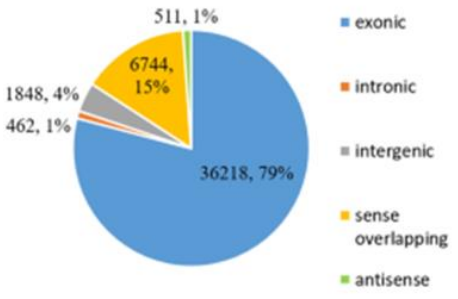


a)

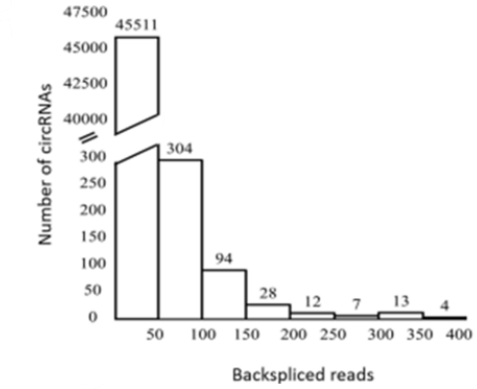


b)

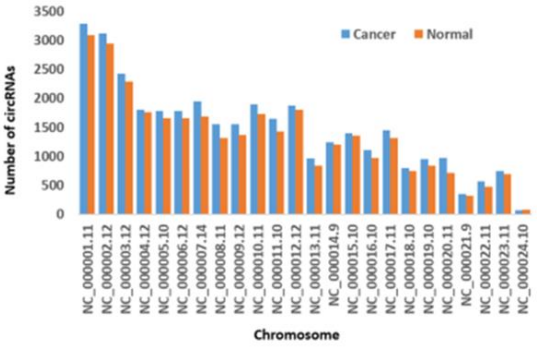


c)

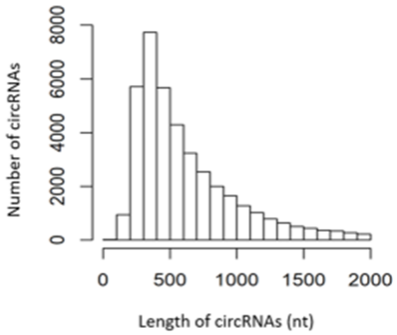


d)

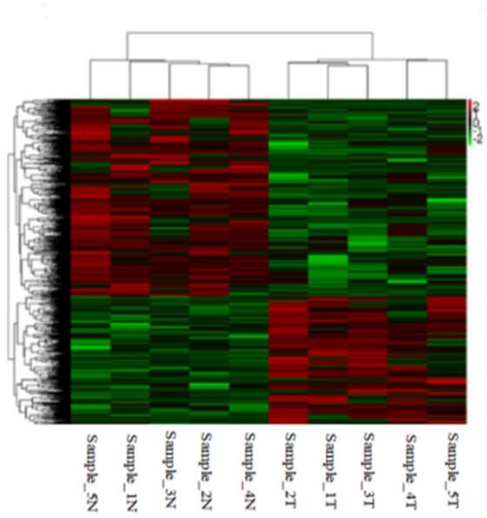


e)

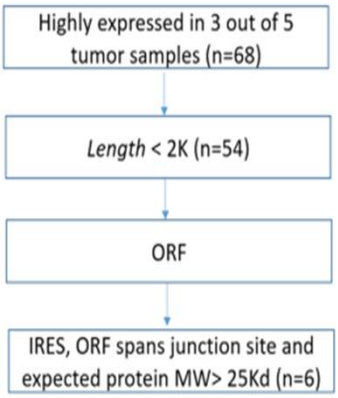


f)

**Figure 1 .**Profile of differentially expressed circRNAs in human gastric cancer (GC) tissues compared to matched adjacent normal tissues.
(a) Counts and proportions of circRNAs derived from various genomic regions. (b) Distribution of identified circRNAs according to the number of supporting back-spliced reads. X-axis: number of back-spliced reads detected for each circRNA in this study; Y-axis: corresponding circRNA count. (c) Chromosomal distribution of circRNAs, revealing no notable differences between cancerous and normal tissue groups. (d) Most circRNAs were shorter than 1500 nucleotides (nt) in length. (e) Hierarchical clustering dendrogram illustrating relationships among samples and differentially expressed circRNAs, with clear separation between normal and cancer tissue expression profiles. (f) Schematic workflow employed to screen for functional circRNAs possessing protein-coding potential in GC.

*CircAXIN1 encodes a novel protein designated AXIN1-295aa*

From the circRNA sequencing results obtained from five paired GC specimens, we identified 68 circRNAs exhibiting high expression levels in at least three samples **(Figure 1f).** Among these, six candidates were chosen for further investigation based on criteria including length, open reading frame (ORF) presence, ORF location, and potential internal ribosome entry sites (IRES). Overexpression vectors for these circRNAs were generated by incorporating a FLAG tag immediately upstream of the stop codon, preserving both the junction site and the intact ORF **(Figure 2a).** Western blot analysis in 293T cells transfected with these six constructs indicated that only circAXIN1 produced a detectable novel protein **(Figure 2b).**

CircAXIN1 is located at chr16:396,147–397,106, consists of exon 2 from its host gene AXIN1, and spans 959 nucleotides. The predicted protein contains 295 amino acids, hence named AXIN1-295aa. To exclude the possibility that absent protein detection in other constructs resulted from poor transfection, qPCR with divergent primers specific to each circRNA confirmed robust overexpression across all six vectors **(Figure 2c).** To verify that AXIN1-295aa is genuinely translated from circAXIN1, we generated mutant and deletion constructs. Disruption of the start codon or removal of downstream sequences flanking the ORF abolished protein expression, demonstrating that translation depends on an intact ORF and proper circRNA circularization **(Figure 2d).** Furthermore, a linear construct designed to express AXIN1-295aa produced a protein with identical molecular weight to that from the circular template **(Figure 2d),** (lanes 5 and 8), confirming the accuracy of our ORF-based prediction.

Subsequently, we examined potential IRES elements in circAXIN1 and pinpointed two candidates: positions 115–257 and 689–838 **(Figure 2e).** These sequences were inserted between mCherry and GFP reporter genes. Both IRESs proved functional, driving GFP expression; however, the second IRES (689–838) displayed stronger activity, yielding higher GFP levels despite reduced mCherry expression **(Figure 2e).** Dual-luciferase reporter assays corroborated these findings in 293T and HFE-145 cells, showing activity for both IRESs but markedly higher for 689–838 **(Figure 2f)**. Notably, full-length sequence appeared necessary for optimal function of IRES 115–257, whereas truncated versions of IRES 689–838 retained substantial activity.

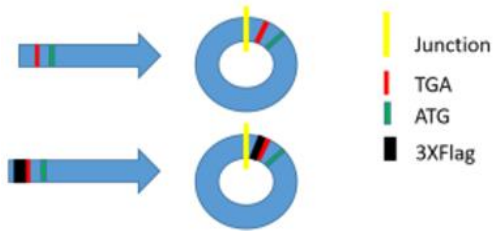


a)

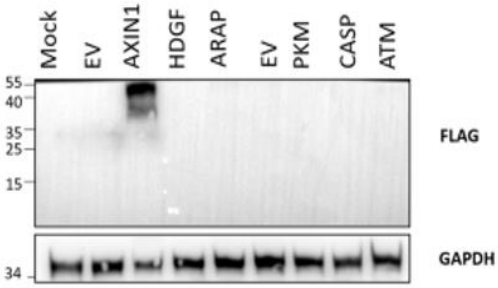


b)

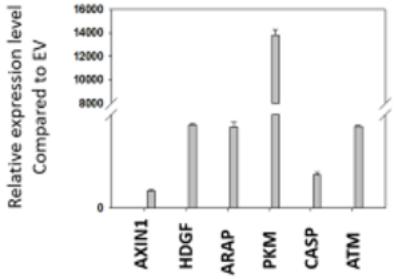


c)

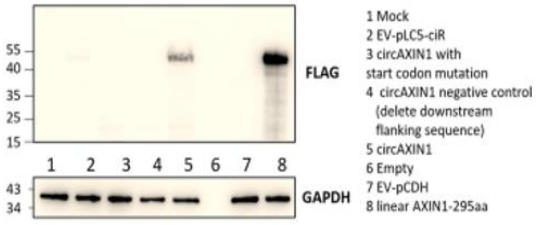


d)

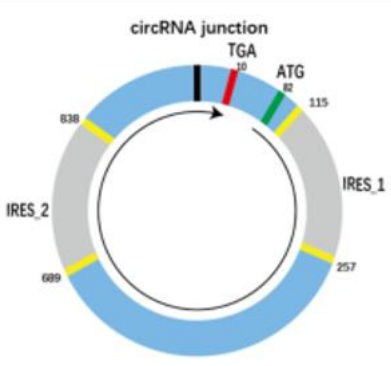


e)

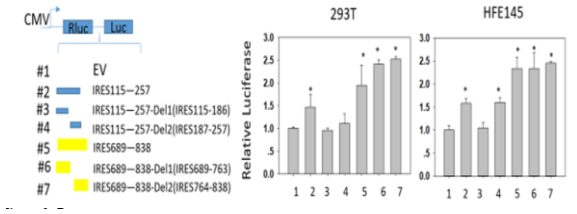


f)

**Figure 2.** CircAXIN1 produces a novel protein termed AXIN1-295aa.

(a) Schematic depicting the design of FLAG-tagged circRNA overexpression vectors. (b) Evidence suggesting that circAXIN1 translates into a new protein, AXIN1-295aa. Western blot analysis of cell lysates from 293T cells transfected with FLAG-tagged circRNA constructs. (c) Successful overexpression of the circRNAs confirmed by quantitative real-time PCR employing divergent primers. (d) Translation of AXIN1-295aa depends on the circular form of circAXIN1. Constructs harboring start codon mutations or deletions in downstream flanking regions failed to produce AXIN1-295aa. A linearized version of the circAXIN1 ORF was inserted into a CMV-driven expression plasmid (linear AXIN1-295aa) as a positive control. (e) Diagram illustrating the positions of the ORF and IRES elements in circAXIN1. Both predicted IRESs exhibited activity. Each IRES was placed between mCherry and GFP reporters, and the resulting constructs were introduced into 293T cells; fluorescence imaging demonstrated expression of both mCherry and GFP. (f) Confirmation of two functional IRESs in circAXIN1. Full-length and truncated IRES sequences were inserted between independent Renilla (Rluc) and Firefly (Luc) luciferase reporters, each with their own start and stop codons. Following transfection into cells, relative luciferase activities were measured.

*CircAXIN1 exhibits high expression levels and correlates positively with lymph node metastasis in gastric cancer (GC)*

To further profile circAXIN1, TPM values for both circAXIN1 and its linear host gene AXIN1 were examined in five GC patient samples from the TCGA dataset (BioProject: PRJNA638934) .Expression of both transcripts was upregulated in GC tissues. As illustrated in **Figure 3a**, the TPM ratio of circAXIN1 to linear AXIN1 ranged from approximately 0.01 to 0.06 and was consistently higher in all five matched GC pairs, indicating relatively abundant circAXIN1 expression. Divergent primers specific to circAXIN1 and convergent primers for linear AXIN1 mRNA were designed **(Figure 3b).** Quantitative PCR analysis showed elevated circAXIN1 levels in several GC cell lines, including AGS, SGC7901, BGC823, and N87. Treatment with RNase R had minimal impact on circAXIN1 abundance across various cell lines, whereas linear AXIN1 mRNA was substantially degraded **(Figure 3c).** Sanger sequencing of the PCR amplicon confirmed that the divergent primers accurately spanned the circAXIN1 junction site **(Figure 3d).** Subcellular localization of circAXIN1 was assessed through fractionation of nuclear and cytoplasmic RNA followed by PCR, as well as fluorescence in situ hybridization (FISH). Results indicated predominant cytoplasmic distribution of circAXIN1 **(Figure 3e),** consistent with its potential for translation.

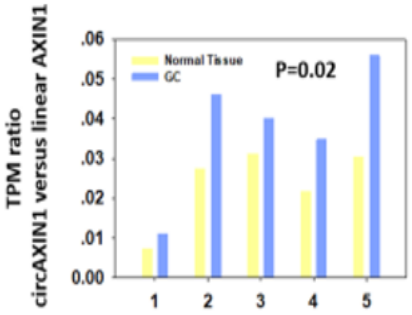


a)

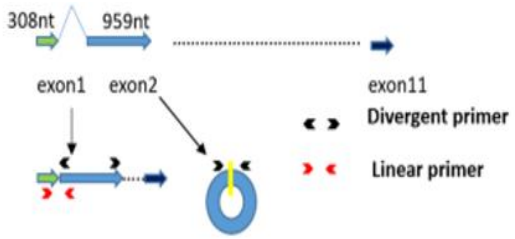


b)

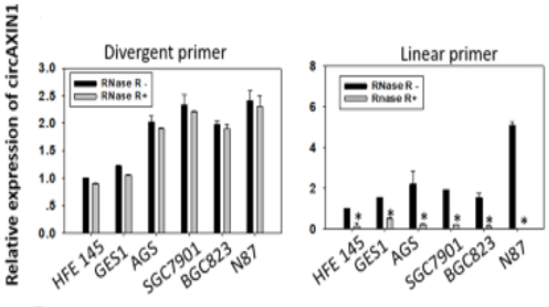


c)

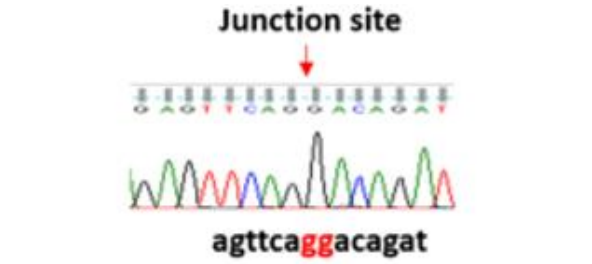


d)

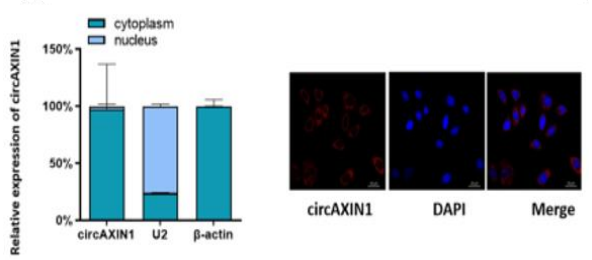


e)

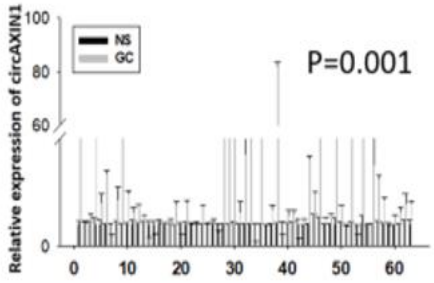


f)

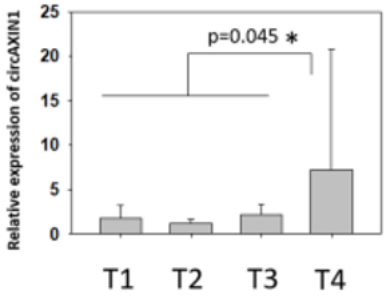


g)

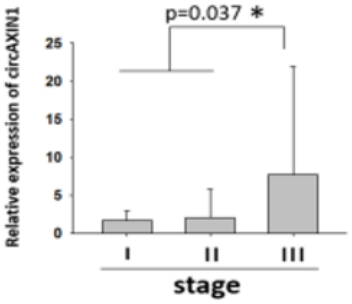


h)

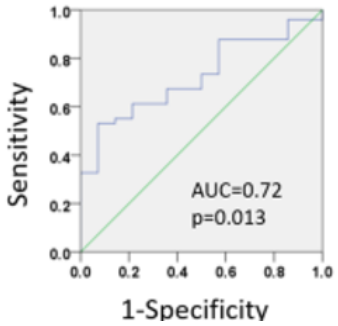


i)

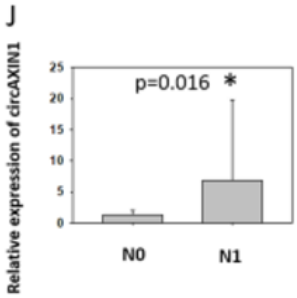


j)

| | circAXIN1 | | |
|---|---|---|---|
| | High | Low | $X^2$ test |
| Lymph Node Metastasis | | | |
| N0 | 1 | 13 | p=0.002 |
| N1 | 26 | 23 | |

k)

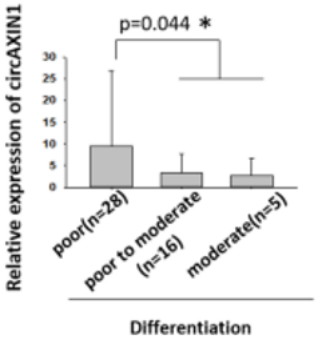


l)

**Figure 3.** Analysis and characterization of circAXIN1 a. In GC samples from the ATGC database, the transcript per million (TPM) ratio of circAXIN1 relative to linear AXIN1 is elevated. b. Diagram showing the genomic structure of AXIN1. CircAXIN1 arises from head-to-tail splicing of exon 2 of AXIN1. Divergent primers were designed to specifically detect circAXIN1, while convergent primers targeted linear AXIN1. c.

CircAXIN1 is expressed at higher levels in GC cell lines compared to normal gastric epithelial cells. RNase R treatment confirms that circAXIN1 is resistant, whereas linear AXIN1 is degraded. d. The back-splice junction of circAXIN1 was validated by Sanger sequencing using divergent primers. e. CircAXIN1 predominantly localizes to the cytoplasm. Left: Quantitative PCR of cytoplasmic and nuclear fractions shows cytoplasmic enrichment, with U2 as the nuclear marker and β-actin as the cytoplasmic control. Right: FISH using junction-specific probes corroborates cytoplasmic localization. f. CircAXIN1 expression is significantly higher in GC tissues than in normal gastric tissues ($p = 0.001$). g. Expression levels of circAXIN1 are elevated in T4 tumors compared to T1–T3, suggesting a correlation with tumor invasion depth ($p = 0.045$). h. Based on AJCC staging, circAXIN1 expression is increased in stage III tumors relative to stages I and II, indicating a link with tumor progression ($p = 0.037$). i. ROC analysis for circAXIN1 expression in GC with or without lymph node metastasis shows an AUC of 0.72 ($p = 0.013$) with a cutoff value of 1.899, indicating its predictive value for lymph node metastasis. j. CircAXIN1 levels are significantly higher in tumors exhibiting lymph node metastasis ($p = 0.016$). k. A positive correlation exists between circAXIN1 expression and lymph node metastasis ($p = 0.002$). l. Among GC tumors with lymph node involvement, circAXIN1 is most highly expressed in poorly differentiated tumors compared to moderately or moderately-to-poorly differentiated tumors, linking elevated expression with poor differentiation. These findings indicate that circAXIN1 is markedly upregulated in gastric cancer, particularly in advanced-stage tumors, and is closely associated with both invasion depth and lymph node metastasis, highlighting its potential as a prognostic marker.

*Characterization of AXIN1-295aa*

To characterize AXIN1-295aa, we carried out mass spectrometry (MS) after overexpressing FLAG-tagged circAXIN1 and performing immunoprecipitation. First, we confirmed the expression and successful pull-down of the FLAG-tagged protein using immunoblotting with an anti-FLAG antibody. Protein lysates were separated by SDS-PAGE, and gel slices corresponding to 25–55 kDa were subjected to MS analysis. The detected peptides matched sequences encoded by circAXIN1. Given that full-length AXIN1 is approximately 110 kDa, the identification of peptides in the 25–55 kDa range indicates that they are derived from circAXIN1 rather than canonical AXIN1.

To further validate these findings, antibodies recognizing the N-terminal region of AXIN1 were obtained from CST (AXIN1 (C7B12) rabbit mAb #3323) and US Biological (A4747-01A). MS was also performed on immunoprecipitates obtained with the A4747-01A antibody in non-transfected cells to detect endogenously produced AXIN1-295aa. Gel fragments from 25–55 kDa were analyzed, and multiple amino acid sequences corresponding to AXIN1-295aa were identified. Notably, the sequence "SSRRYSEGREFRTD," encoded uniquely by circAXIN1 and absent in canonical AXIN1, was detected, confirming the presence of the endogenously expressed AXIN1-295aa protein.

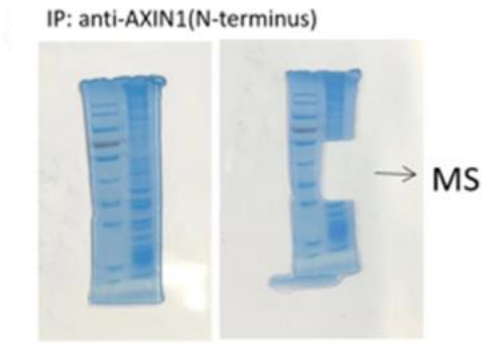


a)

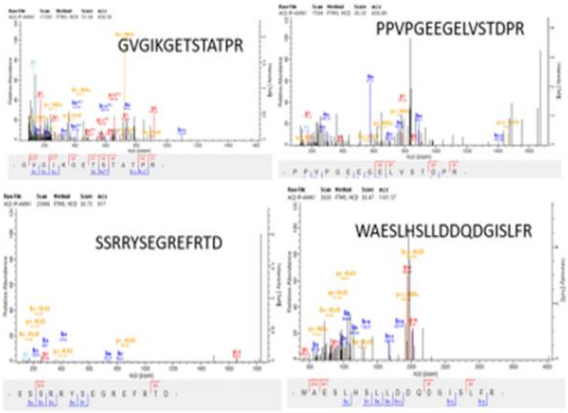


b)

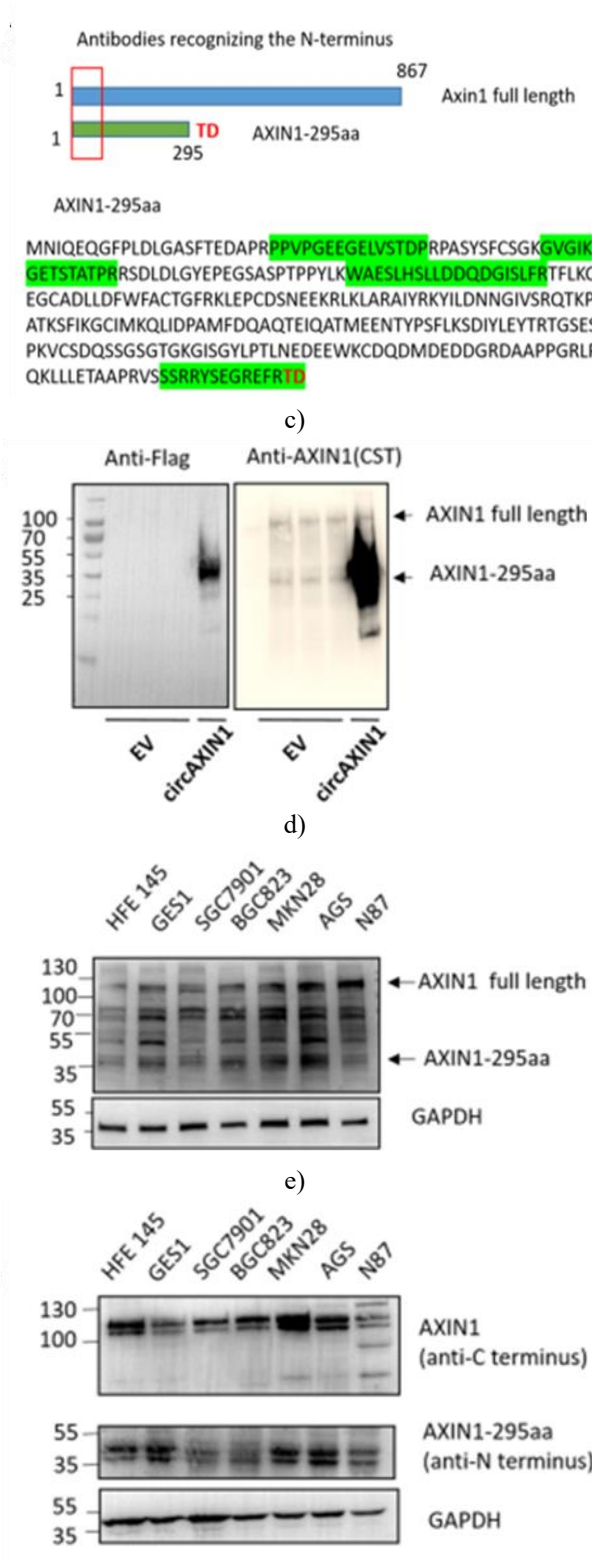


**Figure 4.** AXIN1-295aa Characterization. a. Endogenous AXIN1-295aa was detected via immunoprecipitation using an antibody against the N-terminal region of AXIN1, followed by SDS-PAGE and mass spectrometry of gel fragments from 25–55 kDa. b. Mass spectrometry identified peptides matching AXIN1-295aa. c. AXIN1-295aa shares similarity with the N-terminal portion of full-length AXIN1 but differs by two amino acids at positions 294–295. The unique "TD" sequence is encoded by circAXIN1 and is absent in full-length AXIN1. Commercial antibodies targeting the N-terminal AXIN1 region were used for detection. d. The N-terminal AXIN1 antibody successfully recognized both endogenous and overexpressed AXIN1-295aa. Left: FLAG-tagged AXIN1-295aa was detected using an anti-FLAG antibody. Right: The N-terminal AXIN1 antibody detected full-length AXIN1 as well as AXIN1-295aa, confirming expression from circAXIN1. e. Using the CST N-terminal AXIN1 antibody, both full-length AXIN1 and AXIN1-295aa were observed in GC cell lines. AXIN1-295aa expression was higher in MKN28 and AGS cells compared with the normal HFE145 line. The abundance of AXIN1-295aa was comparable to full-length AXIN1 in several GC lines, supporting translation of circAXIN1. f. A C-terminal AXIN1 antibody and a US Biological N-terminal AXIN1 antibody were used to detect full-length AXIN1 and AXIN1-295aa, respectively, confirming their distinct sizes and presence in GC cells.
Transfection of FLAG-tagged AXIN1-295aa in 293T cells confirmed that the CST N-terminal AXIN1 antibody recognizes both the full-length protein and AXIN1-295aa, consistent with the anti-FLAG signal. Moreover, this antibody detected endogenous AXIN1-295aa in GC cell lines, supporting its origin from circAXIN1.

*CircAXIN1 drives gastric cancer progression via AXIN1-295aa*

To determine the functional role of circAXIN1 in GC, siRNAs targeting the back-splice junction of circAXIN1 were designed. Three siRNAs effectively reduced circAXIN1 levels without affecting linear AXIN1 mRNA **(Figure 5a).** Knockdown of circAXIN1 also lowered AXIN1-295aa protein levels, while full-length AXIN1 remained unchanged **(Figure 5b)** in AGS and N87 cells.

EdU assays showed that circAXIN1 depletion slowed the proliferation of AGS and N87 cells compared with controls **(Figure 5b)**. Transwell migration assays with mitomycin pretreatment and wound healing assays demonstrated reduced cell motility after circAXIN1 knockdown, indicating that decreased migration was not due to proliferation changes **(Figure 5c)** (upper panel, 5d). Similar trends were observed in N87 cells. Suppression of circAXIN1 also impaired invasive capacity **(Figure 5c)** (lower panel) and colony-forming ability **(Figure 5e),** demonstrating that circAXIN1 promotes multiple malignant phenotypes in GC through AXIN1-295aa.

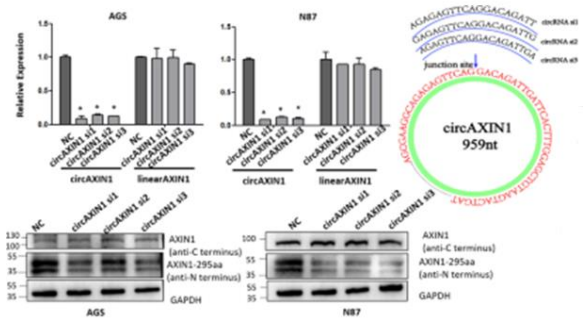


a)

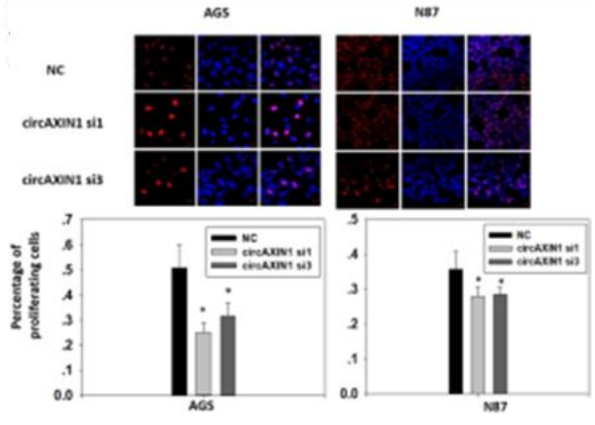


b)

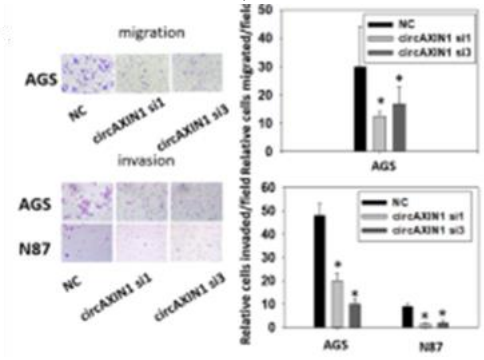


c)

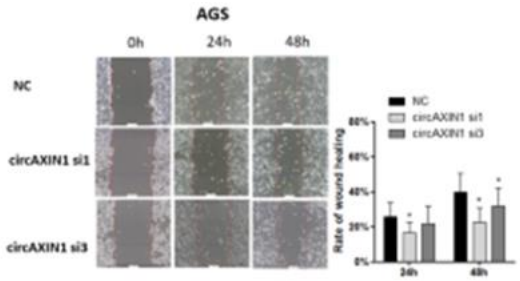


d)

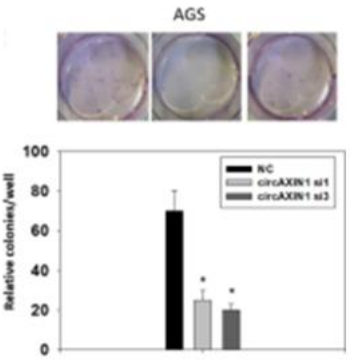


e)

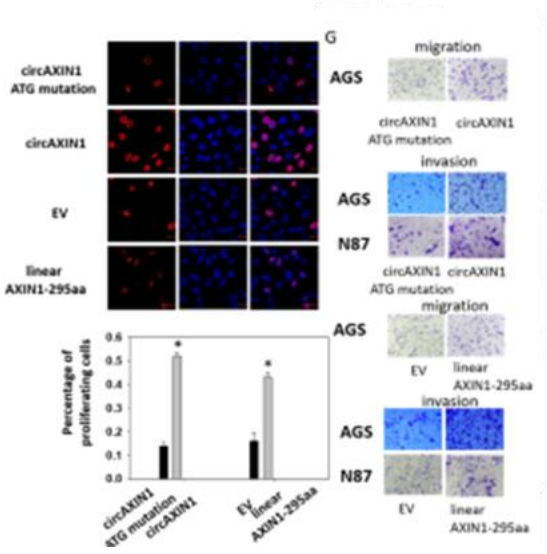


f)

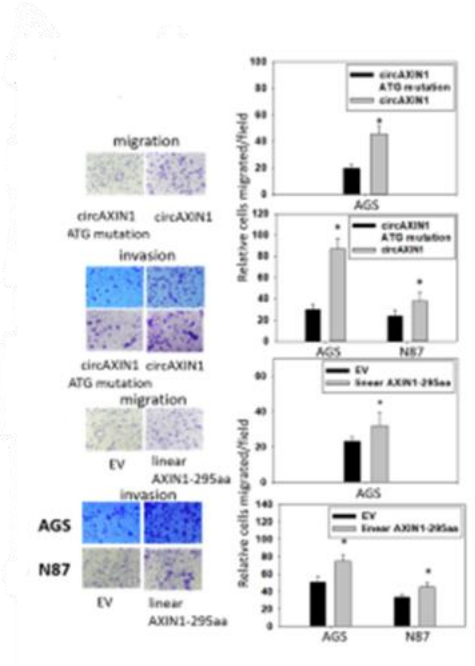


g)

h)

**Figure 5.** Functional analysis of circAXIN1. a. Three specific siRNAs targeting circAXIN1 efficiently reduced both its RNA and protein levels, while linear AXIN1 expression remained unchanged. The diagram indicates the junction site of circAXIN1 targeted by these siRNAs. b. In EdU assays, AGS and N87 cells transfected with circAXIN1 siRNA1 or siRNA3 showed significantly decreased proliferation. c. CircAXIN1 knockdown impaired cell migration in AGS cells (pretreated with 10 μg/mL mitomycin for 1 hour) and reduced the invasive capacity of both AGS and N87 cells. d. Wound healing assays demonstrated that migration of AGS cells was inhibited following circAXIN1 siRNA transfection under mitomycin treatment. e. Colony formation was significantly suppressed in AGS cells following circAXIN1 knockdown. f–h. Conversely, overexpression of circAXIN1 or linear AXIN1-295aa enhanced proliferation (f), invasion (g), and migration (g–h) in AGS and N87 cells. Migration assays in AGS cells included 10 μg/mL mitomycin pretreatment for 1 hour, 48 hours post-transfection. EV represents the empty vector control.

To further explore AXIN1-295aa function independently of circAXIN1, circAXIN1 expression was silenced while AXIN1-295aa was reintroduced via a linear overexpression plasmid. Repressing circAXIN1 reduced proliferation in AGS and N87 cells, but this effect was rescued by AXIN1-295aa expression **(Figure 6a).** Similarly, migration and invasion were suppressed upon circAXIN1 knockdown, and re-expression of linear AXIN1-295aa restored these capabilities **(Figure 6b)**. In wound healing assays, linear AXIN1-295aa reversed the migration inhibition caused by circAXIN1 silencing, demonstrating that AXIN1-295aa mediates the pro-migratory effect of circAXIN1 **(Figure 6c)**. Furthermore, AXIN1-295aa re-expression rescued the reduction in colony formation induced by circAXIN1 knockdown **(Figure 6d)**.

Together, these results indicate that circAXIN1 exerts oncogenic effects in gastric cancer primarily through its encoded protein, AXIN1-295aa.

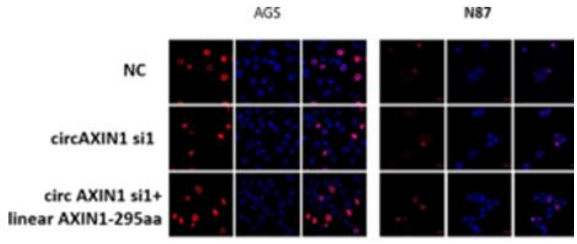


a)

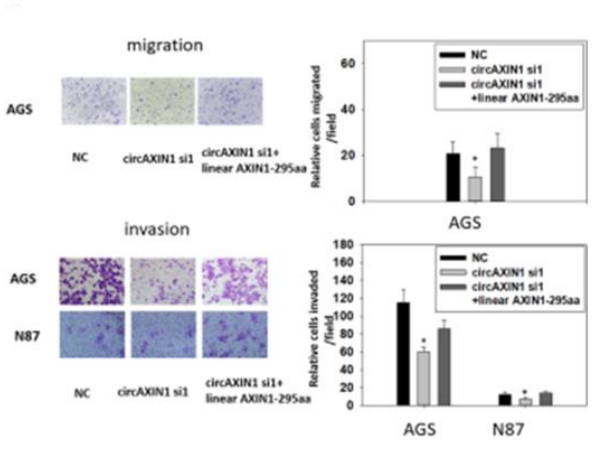


b)

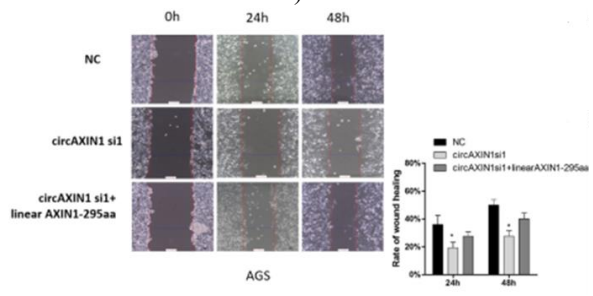


c)

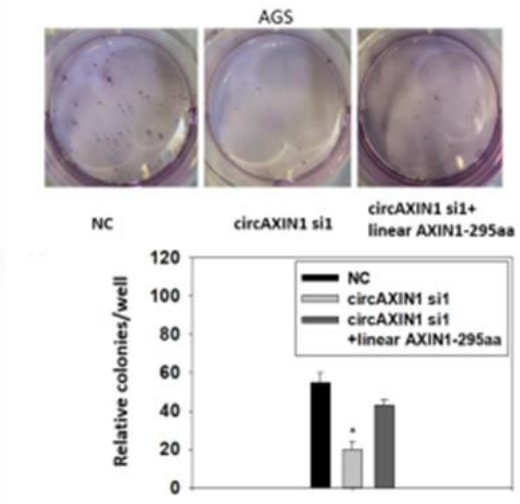


d)

**Figure 6.** AXIN1-295aa Restores Function After circAXIN1 Knockdown. a. Proliferation of AGS and N87 cells was reduced by circAXIN1 siRNA, but co-expression of linear AXIN1-295aa restored cell growth. b. Migration of AGS cells (pretreated with 10 μg/mL mitomycin for 1 hour) and invasion of AGS and N87 cells were suppressed following circAXIN1 silencing; these inhibitory effects were reversed when linear AXIN1-295aa was reintroduced. c. In wound healing assays, the migration deficit caused by circAXIN1 knockdown in AGS cells was rescued by linear AXIN1-295aa, 48 hours after transfection. d. Colony formation, which was impaired by circAXIN1 siRNA in AGS cells, recovered upon linear AXIN1-295aa expression.

*AXIN1-295aa competes with AXIN1 for APC binding*

AXIN1-295aa shares 98% sequence identity with the parental AXIN1 protein, including the entire RGS domain that mediates APC binding, while lacking the β-catenin interaction region **(Figure 7a).** Structural prediction using the fold recognition method PHYRE [23] indicated that AXIN1-295aa contains two main domains: the tankyrase-binding N-terminal segment (TKNS, blue) and the RGS domain (green) **(Figure 7a),** (lower left). The SAMP motif of APC, a 25-amino-acid sequence, is known to directly bind the RGS domain of AXIN1 [22]. Using ZDOCK [24], the interaction between AXIN1-295aa and the SAMP motif was modeled (red line) **(Figure 7a),** demonstrating that AXIN1-295aa can bind APC via its RGS domain. These results suggest that AXIN1-295aa competes with full-length AXIN1 for APC binding, potentially acting as a dominant-negative modulator of AXIN1 activity.

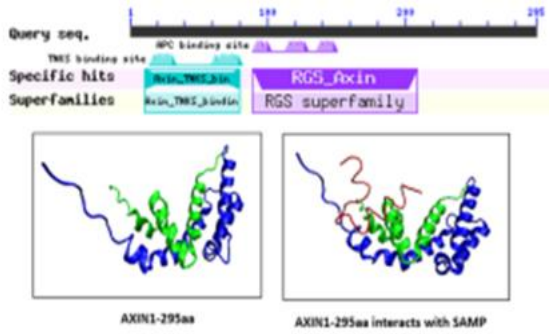


a)

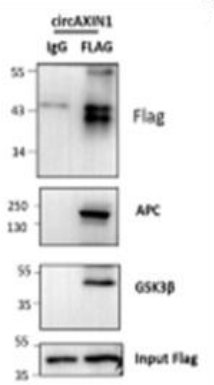


b)

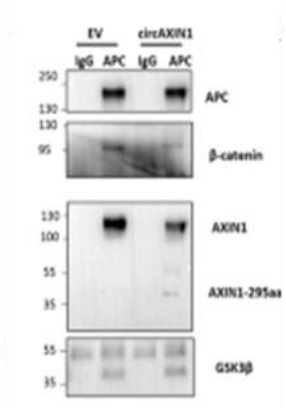


c)

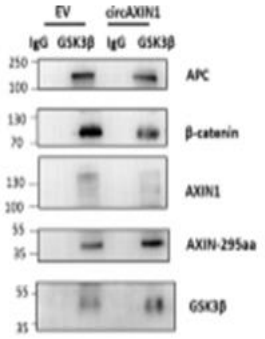


d)

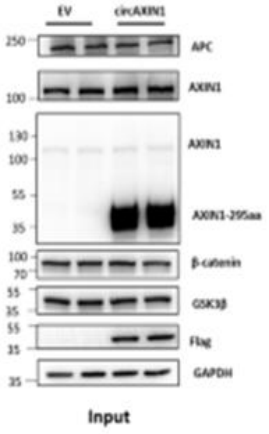


e)

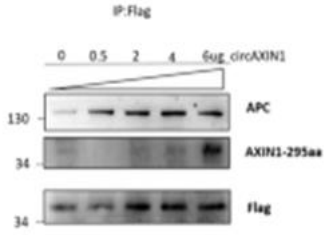


f)

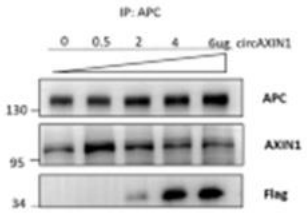


g)

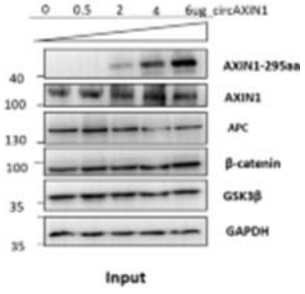


h)

**Figure 7.** AXIN1-295aa Competes with AXIN1 for APC Binding. a. Sequence alignment confirmed that AXIN1-295aa retains the RGS domain. Structural modeling using PHYRE and ZDOCK illustrated the predicted 3D structure of AXIN1-295aa (left) and the simulated binding interface with the SAMP domain of APC (right, red line), which normally interacts with full-length AXIN1.b–d. Co-immunoprecipitation (co-IP) assays were performed to examine interactions among AXIN1-295aa, AXIN1, APC, β-catenin, and GSK3β. b. FLAG-tagged AXIN1-295aa pulled down APC and GSK3β in 293T cells, indicating direct interaction. c. Overexpression of circAXIN1 reduced the binding of APC to AXIN1 and β-catenin while increasing its association with AXIN1-295aa, demonstrating competitive binding of AXIN1-295aa to APC. d. The interaction between GSK3β and β-catenin decreased, whereas GSK3β binding to AXIN1-295aa increased under circAXIN1 overexpression, indicating AXIN1-295aa participates in the destruction complex. e. Immunoblotting of whole-cell lysates showed that the expression of APC, AXIN1, GSK3β, and β-catenin remained largely unchanged upon circAXIN1 transfection, while AXIN1-295aa was expressed, confirming that altered interactions were not due to changes in protein levels. f–g. Increasing doses of AXIN1-295aa were transfected into 293T cells, followed by co-IP to evaluate binding with APC. f. Higher levels of AXIN1-295aa led to greater amounts of

APC being pulled down. g. With increasing AXIN1-295aa expression, APC binding to full-length AXIN1 decreased, while binding to AXIN1-295aa increased, confirming competitive interaction. h. Dose-dependent overexpression of AXIN1-295aa was confirmed in total cell lysates, while the levels of AXIN1, APC, GSK3β, and β-catenin remained stable, validating that the observed effects on binding were due to competition rather than changes in protein abundance.

*AXIN1-295aa activates the Wnt/β-catenin signaling pathway*

Given that AXIN1-295aa competes with AXIN1 for APC binding, we hypothesized that AXIN1-295aa could activate the canonical Wnt/β-catenin signaling pathway. Using a TOPFlash reporter assay, overexpression of circAXIN1 significantly stimulated Wnt/β-catenin activity in both 293T and AGS cells **(Figure 8a)**. Similarly, linear AXIN1-295aa expression also enhanced Wnt signaling **(Figure 8b)**, whereas knockdown of circAXIN1 using siRNAs reduced TCF-dependent transcription **(Figure 8c)**, indicating that both circAXIN1 and its encoded protein AXIN1-295aa activate the Wnt/β-catenin pathway.

To further validate this, we examined β-catenin localization. CircAXIN1 silencing decreased both cytoplasmic and nuclear β-catenin levels **(Figure 8d)**. Confocal immunofluorescence corroborated these results: elevated circAXIN1 or treatment with a Wnt agonist promoted β-catenin nuclear translocation, while circAXIN1 siRNA or the Wnt inhibitor XAV939 reduced nuclear β-catenin **(Figure 8e).**

Overexpression of circAXIN1 increased the expression of specific Wnt target genes, including Met, c-Myc, LEF1, MMP7, TCF1, CD44, and c-Jun, whereas some targets like cyclinD1 remained unchanged, suggesting selective activation of Wnt-dependent genes **(Figure 8f).** Conversely, circAXIN1 knockdown decreased mRNA and protein levels of Wnt-responsive genes such as c-Myc, c-Jun, CD44, Met, and cyclinD1 **(Figures 8g and 8h).**

To confirm that β-catenin directly regulates these genes, we performed ChIP assays for c-Jun, c-Myc, and CD44. CircAXIN1 overexpression enhanced β-catenin binding to their promoters **(Figure 8i)**. To determine whether AXIN1-295aa mediates this effect, we co-transfected circAXIN1 siRNA with linear AXIN1-295aa. CircAXIN1 silencing suppressed β-catenin-dependent transcription, but this inhibition was rescued by AXIN1-295aa **(Figure 8j).** Likewise, Wnt target genes downregulated by circAXIN1 knockdown were restored upon AXIN1-295aa expression **(Figure 8k),** demonstrating that circAXIN1 activates the canonical Wnt/β-catenin pathway primarily through AXIN1-295aa.

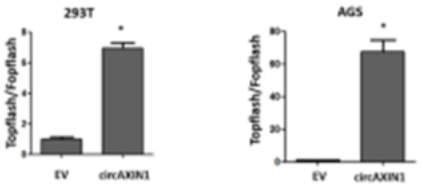


a)

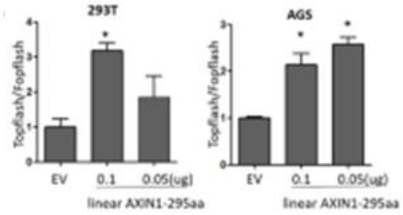


b)

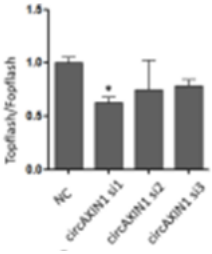


c)

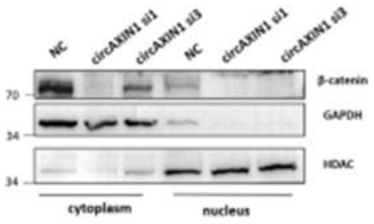


d)

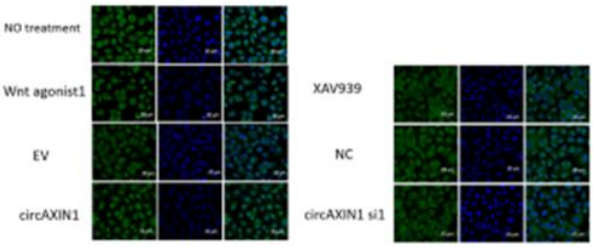


e)

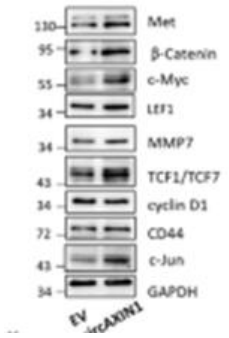


f)

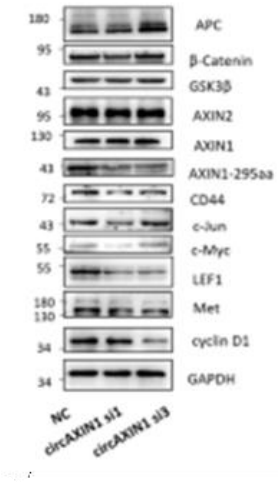


g)

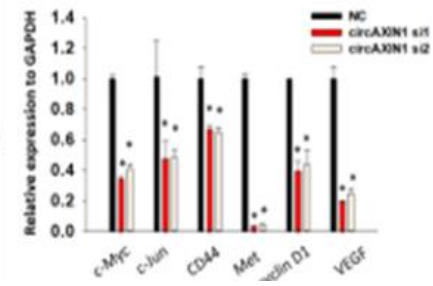


h)

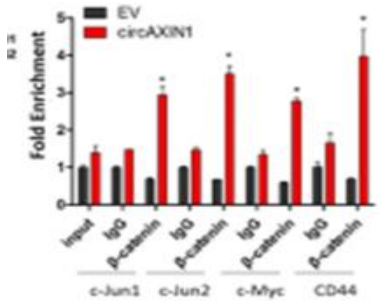


i)

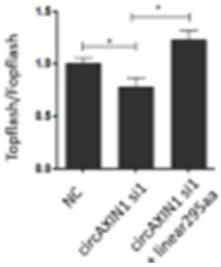


j)

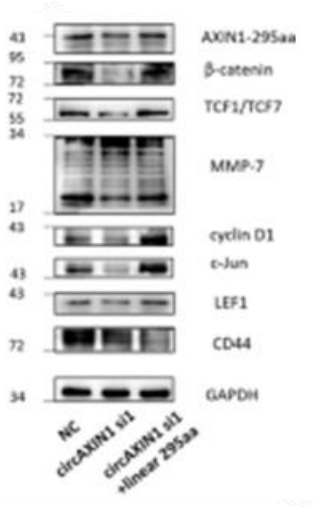


k)

**Figure 8.** CircAXIN1 Activates the Wnt/β-Catenin Pathway. a–b. Both circAXIN1 and AXIN1-295aa enhance Wnt/β-catenin-dependent transcription, as demonstrated by Topflash/Fopflash reporter assays in 293T and AGS cells. CircAXIN1 overexpression (a) and linear AXIN1-295aa expression (b) both increased reporter activity. c. Knockdown of circAXIN1 via individual siRNAs in 293T cells reduced TCF-dependent transcription, indicating suppression of Wnt signaling. d. CircAXIN1 silencing decreased β-catenin levels in both the cytoplasm and nucleus, confirming reduced Wnt pathway activation. e. Immunofluorescence analysis showed that circAXIN1 overexpression promoted nuclear translocation of β-catenin, whereas circAXIN1 siRNA inhibited nuclear accumulation. Wnt agonist1 and XAV939 were used as positive and negative controls, respectively. f. Overexpression of circAXIN1 upregulated Wnt target genes, indicating activation of downstream signaling. g–h. Transfection with circAXIN1 siRNAs reduced expression of Wnt/β-catenin target genes at the protein (g) and mRNA (h) levels, including c-Myc, c-Jun, CD44, Met, cyclinD1, and VEGF. i. ChIP assays

confirmed that circAXIN1 overexpression increased binding of β-catenin to TCF-dependent promoters of c-Jun, c-Myc, and CD44. Regions C-Jun1/2 represent distinct promoter regions of c-Jun. j. Co-transfection of linear AXIN1-295aa with circAXIN1 siRNA restored the reduction in Topflash activity caused by circAXIN1 knockdown. k. Similarly, linear AXIN1-295aa rescued the downregulation of Wnt target genes caused by circAXIN1 siRNA, confirming that circAXIN1 activates Wnt/β-catenin signaling through AXIN1-295aa.

*CircAXIN1 promotes gastric cancer in vivo*

To examine the in vivo oncogenic role of circAXIN1, AGS cells were subcutaneously injected into mice to establish xenograft tumors. Cholesterol-conjugated circAXIN1-specific siRNAs were locally administered twice weekly for three weeks. Tumors in mice treated with circAXIN1 siRNA showed significantly smaller volumes and weights compared with controls **(Figures 9a and 9b)**. CircAXIN1 knockdown in tumors was confirmed by reduced RNA levels **(Figure 9c).**

Immunohistochemistry revealed decreased expression of Ki67, TCF-1, β-catenin, c-Jun, and Met in circAXIN1 siRNA-treated tumors, demonstrating inhibited proliferation and Wnt signaling **(Figure 9d).** Furthermore, tail vein injection experiments showed that circAXIN1 silencing significantly reduced lung metastatic colonies **(Figure 9e).**

These results indicate that circAXIN1 promotes gastric cancer growth and metastasis in vivo, confirming its oncogenic function.

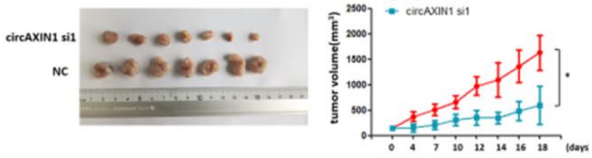


a)

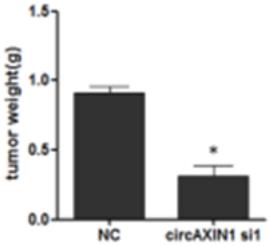


b)

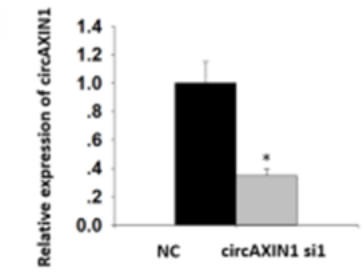


c)

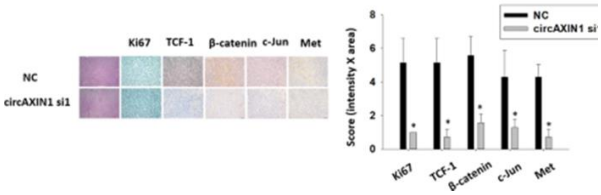


d)

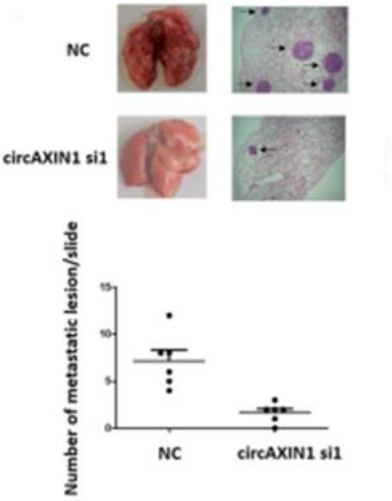


e)

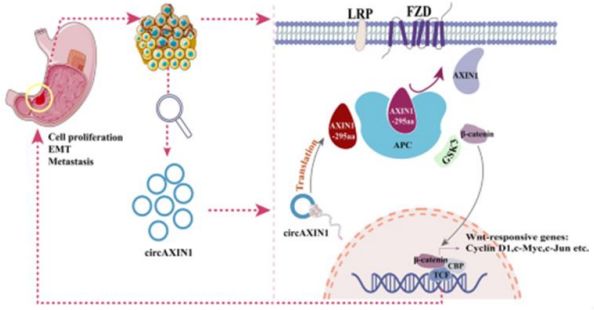


f)

**Figure 9.** Inhibition of circAXIN1 Suppresses Gastric Cancer Growth and Metastasis in Vivo. a–b. Subcutaneous xenograft tumors formed by AGS cells were treated with cholesterol-conjugated circAXIN1 siRNA or negative control (NC) twice weekly for three

weeks. Tumor growth was significantly suppressed in the circAXIN1-siRNA group, as shown by reduced tumor volumes (a) and weights (b, n = 7). c. CircAXIN1 expression in resected tumors was effectively reduced by siRNA treatment. d. Immunohistochemical analyses revealed that Ki67, TCF-1, β-catenin, c-Jun, and Met were significantly downregulated in circAXIN1-siRNA-treated tumors compared to controls. e. Tail vein injection of AGS cells followed by circAXIN1 siRNA administration markedly decreased lung metastases, as quantified by H&E staining. f. Graphical abstract summarizing the study: circAXIN1 is upregulated in gastric cancer and correlates with lymph node metastasis. CircAXIN1 encodes AXIN1-295aa, which competitively binds APC, releases β-catenin for nuclear translocation, and activates canonical Wnt signaling, thereby promoting proliferation and migration.

Our results demonstrate that circAXIN1 is highly expressed in GC tissues and encodes a novel protein, AXIN1-295aa. Overexpression of circAXIN1 or AXIN1-295aa enhanced GC cell proliferation, migration, and invasion, while their knockdown inhibited these malignant phenotypes both in vitro and in vivo. Mechanistically, AXIN1-295aa competes with AXIN1 for APC binding within the destruction complex, resulting in activation of the Wnt/β-catenin pathway and promoting GC progression **(Figure 9f).**

Although circRNAs were discovered decades ago, their biological significance was overlooked until the advent of high-throughput sequencing, which revealed that circRNAs are abundant, conserved, and widespread in eukaryotic cells [26–28]. They perform important regulatory functions [29], acting as microRNA sponges or protein scaffolds, and can also encode functional peptides [30–32]. While many circRNAs have low expression or few miRNA binding sites, recent studies indicate that circRNAs, lncRNAs, and even pri-miRNAs can encode bioactive peptides. For instance, the 34-amino-acid peptide Dworf from lncRNA Dworf enhances muscle contractility [33], and plant miRNA-derived peptides regulate root development [34]. Functional circRNA-derived proteins include ZNF609 from circ-ZNF609 [35], FBXW7-185aa from circ-FBXW7 [36], and β-catenin-370aa from circβ-catenin [37]. In this study, circAXIN1 was found to encode AXIN1-295aa, promoting GC progression.

Criteria for identifying coding circRNAs include: high differential expression in GC, a complete ORF spanning the junction site, relevance of the parental gene to cancer, and experimental verification of protein expression. Many peptides from circRNAs may remain undetected if only junction-spanning ORFs are considered. Ribosome profiling is the most reliable method to identify coding circRNAs, though stringent conditions may miss some, as observed for circAXIN1.

Most circRNA-derived proteins share N-terminal sequences with parental proteins, potentially acting as decoys or competitors. For example, AKT3-174aa competes with AKT3 to negatively regulate PI3K/AKT signaling [10]. CircRNA translation can be enhanced under stress or during tumor development, a hypothesis worth further study.

AXIN1 serves as the central scaffold in the β-catenin destruction complex, interacting with APC, β-catenin, CKα, and GSK3β [14, 38]. Typically a tumor suppressor [39–42], AXIN1 is rate-limiting in Wnt regulation [43]. AXIN1-295aa contains only the APC-binding RGS domain but, through APC, also associates with β-catenin and GSK3β, saturating APC and preventing formation of the canonical destruction complex, thereby allowing β-catenin nuclear translocation and activation of downstream genes.

CircAXIN1's high stability makes it a promising biomarker [44]. Its expression correlates with tumor invasion, differentiation, stage, and lymph node metastasis, suggesting prognostic potential, though larger studies are needed. CircAXIN1 siRNA demonstrated therapeutic efficacy in xenograft and metastasis models with minimal adverse effects, highlighting potential clinical applications [45].

## Conclusion

This study establishes that circAXIN1 is translatable and oncogenic in GC. CircAXIN1 encodes AXIN1-295aa, which competitively binds APC, induces β-catenin nuclear translocation, activates canonical Wnt signaling, and promotes proliferation and migration, revealing a novel mechanism driving GC progression.

**Acknowledgments:** We appreciate Dr. Jessica Tamanini for language editing of the manuscript and scientific comments.

**Conflict of Interest:** None

**Financial Support:** This work was supported in part by National Natural Science Foundation of China

(81772592, 31601028, 81871969, 82173290, 82172946); Medical Science and Technology Research Foundation of Guangdong Province (A2019211); Shenzhen Basic Research Fund (JCYJ20190808163801777); Shenzhen University Talent Program (000324), High Quality University Construction 2nd phase (860–00000210); National Key Research and Development Program of China (2016YFB0201305); Youth Talent Support Program in Medical Center Shenzhen University.

**Ethics Statement:** None

**References**

1. Chen LL. The expanding regulatory mechanisms and cellular functions of circular RNAs. Nat Rev Mol Cell Biol. 2020;21:475–90.
2. Zhang XO, Dong R, Zhang Y, Zhang JL, Luo Z, Zhang J, et al. Diverse alternative back-splicing and alternative splicing landscape of circular RNAs. Genome Res. 2016;26:1277–87.
3. Zhang XO, Wang HB, Zhang Y, Lu X, Chen LL, Yang L. Complementary sequence-mediated exon circularization. Cell. 2014;159:134–47.
4. Qu S, Yang X, Li X, Wang J, Gao Y, Shang R, et al. Circular RNA: a new star of noncoding RNAs. Cancer Lett. 2015;365:141–8.
5. Li X, Yang L, Chen LL. The biogenesis, functions, and challenges of circular RNAs. Mol Cell. 2018;71:428–42.
6. Li J, Ma M, Yang X, Zhang M, Luo J, Zhou H, et al. Circular HER2 RNA positive triple negative breast cancer is sensitive to Pertuzumab. Mol Cancer. 2020;19:142.
7. Xing Y, Zha WJ, Li XM, Li H, Gao F, Ye T, et al. Circular RNA circ-Foxo3 inhibits esophageal squamous cell cancer progression via the miR-23a/PTEN axis. J Cell Biochem. 2020;121:2595–605.
8. Zheng X, Chen L, Zhou Y, Wang Q, Zheng Z, Xu B, et al. A novel protein encoded by a circular RNA circPPP1R12A promotes tumor pathogenesis and metastasis of colon cancer via hippo-YAP signaling. Mol Cancer. 2019;18:47.
9. Qian L, Yu S, Chen Z, Meng Z, Huang S, Wang P. The emerging role of circRNAs and their clinical significance in human cancers. Biochim Biophys Acta Rev Cancer. 2018;1870:247–60.
10. Xia X, Li X, Li F, Wu X, Zhang M, Zhou H, et al. A novel tumor suppressor protein encoded by circular AKT3 RNA inhibits glioblastoma tumorigenicity by competing with active phosphoinositide-dependent Kinase-1. Mol Cancer. 2019;18:131.
11. Chen W, Zheng R, Baade PD, Zhang S, Zeng H, Bray F, et al. Cancer statistics in China, 2015. CA Cancer J Clin. 2016;66:115–32.
12. Zhan T, Rindtorff N, Boutros M. Wnt signaling in cancer. Oncogene. 2017;36:1461–73.
13. Nusse R, Clevers H. Wnt/beta-catenin signaling, disease, and emerging therapeutic modalities. Cell. 2017;169:985–99.
14. Stamos JL, Weis WI. The beta-catenin destruction complex. Cold Spring Harb Perspect Biol. 2013;5:a007898.
15. Deng S, Zhang X, Qin Y, Chen W, Fan H, Feng X, et al. Cheng Y, et al: miRNA-192 and -215 activate Wnt/beta-catenin signaling pathway in gastric cancer via APC. J Cell Physiol. 2020;235:6218–29.
16. Ji L, Jiang B, Jiang X, Charlat O, Chen A, Mickanin C, et al. The SIAH E3 ubiquitin ligases promote Wnt/beta-catenin signaling through mediating Wnt-induced Axin degradation. Genes Dev. 2017;31:904–15.
17. Clements WM, Wang J, Sarnaik A, Kim OJ, MacDonald J, Fenoglio-Preiser C, et al. Lowy AM: beta-catenin mutation is a frequent cause of Wnt pathway activation in gastric cancer. Cancer Res. 2002;62:3503–6.
18. Peng Y, Zhang X, Feng X, Fan X, Jin Z. The crosstalk between microRNAs and the Wnt/beta-catenin signaling pathway in cancer. Oncotarget. 2017;8:14089–106.
19. Jie M, Wu Y, Gao M, Li X, Liu C, Ouyang Q, et al. CircMRPS35 suppresses gastric cancer progression via recruiting KAT7 to govern histone modification. Mol Cancer. 2020;19:56.
20. Yang F, Hu A, Li D, Wang J, Guo Y, Liu Y, et al. Circ-HuR suppresses HuR expression and gastric cancer progression by inhibiting CNBP transactivation. Mol Cancer. 2019;18:158.
21. Peng Y, Zhang X, Ma Q, Yan R, Qin Y, Zhao Y, et al. MiRNA-194 activates the Wnt/beta-catenin signaling pathway in gastric cancer by targeting the negative Wnt regulator, SUFU. Cancer Lett. 2017;385:117–27.

22. Spink KE, Polakis P, Weis WI. Structural basis of the Axin-adenomatous polyposis coli interaction. EMBO J. 2000;19:2270–9.
23. Kelley LA, Mezulis S, Yates CM, Wass MN, Sternberg MJ. The Phyre2 web portal for protein modeling, prediction and analysis. Nat Protoc. 2015;10:845–58.
24. Pierce BG, Wiehe K, Hwang H, Kim BH, Vreven T, Weng Z. ZDOCK server: interactive docking prediction of protein-protein complexes and symmetric multimers. Bioinformatics. 2014;30:1771–3.
25. Peng Y, Zhang X, Lin H, Deng S, Qin Y, He J, et al. Dual activation of Hedgehog and Wnt/beta-catenin signaling pathway caused by downregulation of SUFU targeted by miRNA-150 in human gastric cancer. Aging (Albany NY). 2021;13:10749–69.
26. Jeck WR, Sorrentino JA, Wang K, Slevin MK, Burd CE, Liu J, et al. Circular RNAs are abundant, conserved, and associated with ALU repeats. RNA. 2013;19:141–57.
27. Guo JU, Agarwal V, Guo H, Bartel DP. Expanded identification and characterization of mammalian circular RNAs. Genome Biol. 2014;15:409.
28. Salzman J, Gawad C, Wang PL, Lacayo N, Brown PO. Circular RNAs are the predominant transcript isoform from hundreds of human genes in diverse cell types. PLoS One. 2012;7:e30733.
29. Memczak S, Jens M, Elefsinioti A, Torti F, Krueger J, Rybak A, et al. Circular RNAs are a large class of animal RNAs with regulatory potency. Nature. 2013;495:333–8.
30. Lei M, Zheng G, Ning Q, Zheng J, Dong D. Translation and functional roles of circular RNAs in human cancer. Mol Cancer. 2020;19:30.
31. Yang Y, Fan X, Mao M, Song X, Wu P, Zhang Y, et al. Extensive translation of circular RNAs driven by N(6)-methyladenosine. Cell Res. 2017;27:626–41.
32. Zheng SL, Li L, Zhang HP. Progress on translation ability of circular RNA. Yi Chuan. 2020;42:423–34.
33. Nelson BR, Makarewich CA, Anderson DM, Winders BR, Troupes CD, Wu F, et al. A peptide encoded by a transcript annotated as long noncoding RNA enhances SERCA activity in muscle. Science. 2016;351:271–5.
34. Lauressergues D, Couzigou JM, Clemente HS, Martinez Y, Dunand C, Becard G, et al. Primary transcripts of microRNAs encode regulatory peptides. Nature. 2015;520:90–3.
35. Legnini I, Di Timoteo G, Rossi F, Morlando M, Briganti F, Sthandier O, et al. Circ-ZNF609 is a circular RNA that can be translated and functions in Myogenesis. Mol Cell. 2017;66:22–37 e29.
36. Yang Y, Gao X, Zhang M, Yan S, Sun C, Xiao F, et al. Novel role of FBXW7 circular RNA in repressing Glioma tumorigenesis. J Natl Cancer Inst. 2018;110:304–15.
37. Liang WC, Wong CW, Liang PP, Shi M, Cao Y, Rao ST, et al. Translation of the circular RNA circbeta-catenin promotes liver cancer cell growth through activation of the Wnt pathway. Genome Biol. 2019;20:84.
38. Nakamura T, Hamada F, Ishidate T, Anai K, Kawahara K, Toyoshima K, et al. Axin, an inhibitor of the Wnt signalling pathway, interacts with beta-catenin, GSK-3beta and APC and reduces the beta-catenin level. Genes Cells. 1998;3:395–403.
39. Mazzoni SM, Fearon ER. AXIN1 and AXIN2 variants in gastrointestinal cancers. Cancer Lett. 2014;355:1–8.
40. Salahshor S, Woodgett JR. The links between axin and carcinogenesis. J Clin Pathol. 2005;58:225–36.
41. Jin LH, Shao QJ, Luo W, Ye ZY, Li Q, Lin SC. Detection of point mutations of the Axin1 gene in colorectal cancers. Int J Cancer. 2003;107:696–9.
42. Khan NP, Pandith AA, Hussain MU, Yousuf A, Khan MS, Wani KA, et al. Novelty of Axin 2 and lack of Axin 1 gene mutation in colorectal cancer: a study in Kashmiri population. Mol Cell Biochem. 2011;355:149–55.
43. Thorvaldsen TE, Pedersen NM, Wenzel EM, Stenmark H. Differential roles of AXIN1 and AXIN2 in Tankyrase inhibitor-induced formation of Degradasomes and beta-catenin degradation. PLoS One. 2017;12:e0170508.
44. Meng S, Zhou H, Feng Z, Xu Z, Tang Y, Li P, et al. CircRNA: functions and properties of a novel potential biomarker for cancer. Mol Cancer. 2017;16:94.
45. Wang S, Zhang K, Tan S, Xin J, Yuan Q, Xu H, et al. Circular RNAs in body fluids as cancer biomarkers: the new frontier of liquid biopsies. Mol Cancer. 2021;20:13.